Translational Oncology 69 (2026) 102802

Contents lists available at ScienceDirect

Translational Oncology

journal homepage: www.elsevier.com/locate/tranon

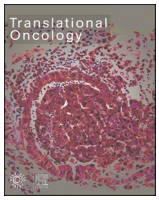

Integrated bioinformatics and experimental validation identifies CLIC6 as a novel tumor suppressor regulating NF-κB signaling and immune microenvironment in nasopharyngeal carcinoma

Zhuo Chen [a,1], Mingxian Li [a,1], Pei Gao [b], Yulin Zhao [a,*]

[a] Department of Rhinology, The First Affiliated Hospital of Zhengzhou University, Zhengzhou, 450052 Henan, China
[b] Department of Otolaryngology Head and Neck Surgery, The First Affiliated Hospital of Zhengzhou University, Zhengzhou, 450052 Henan, China

ARTICLE INFO

Keywords:
Nasopharyngeal carcinoma
Clic6
M1 macrophages
Nf-κb signaling pathway
Tumor microenvironment

ABSTRACT

Background: Nasopharyngeal carcinoma (NPC) is an Epstein-Barr virus–associated malignancy. Tumor-associated macrophages play a pivotal role in NPC development, but molecular mechanisms remain unclear. This study aimed to identify M1 macrophage-associated hub genes and investigate their biological functions in NPC via bioinformatics and experimental validation.

Methods: GSE12452 and GSE53819 datasets were integrated to assess immune cell infiltration using CIBERSORT. WGCNA identified gene modules correlated with M1 macrophages. Hub genes were identified by intersecting differentially expressed genes with module genes, followed by LASSO regression and clinical specimen validation. CCK-8, Transwell assays, and macrophage co-culture systems were used to evaluate CLIC6 effects on NPC cell proliferation, invasion, and M1 polarization. RNA-seq and Western blot were performed to explore downstream mechanisms, with rescue experiments using NF-κB activator or inhibitor.

Results: M1 macrophages were significantly enriched in NPC tissues and negatively correlated with cilia-related gene modules. Six hub genes (MUC16, MS4A8, MUC20, AMIGO1, PHYHD1, CLIC6) were identified, with CLIC6 showing significant downregulation in NPC tissues and cell lines and negative correlation with M1 macrophages. CLIC6 recombinant protein promoted NPC cell proliferation and invasion while inhibiting M1 polarization, whereas CLIC6 silencing produced opposite effects. Mechanistically, CLIC6 suppressed NF-κB signaling by inhibiting IκBα and p65 phosphorylation, confirmed by RNA-seq and Western blot. Functional rescue experiments demonstrated that NF-κB modulation reversed CLIC6-mediated effects.

Conclusion: CLIC6 functions as a tumor suppressor in NPC by inhibiting NF-κB signaling, thereby regulating tumor cell proliferation, invasion, and macrophage polarization. The CLIC6-NF-κB axis represents a potential diagnostic biomarker and therapeutic target for NPC.

Introduction

Nasopharyngeal carcinoma (NPC) is a distinct head and neck malignancy with unique epidemiological characteristics, exhibiting the highest incidence rates in East and Southeast Asia, where over 70% of new cases occur annually [1,2]. Although advances in intensity-modulated radiotherapy and concurrent chemoradiotherapy have improved treatment outcomes for early-stage patients, the prognosis for individuals with recurrent or metastatic disease remains poor, with mortality rates remaining unacceptably high [3,4]. The lack of specific early symptoms and reliable diagnostic biomarkers often leads to delayed diagnosis, highlighting the urgent need for novel molecular targets for early detection and therapeutic intervention [5,6].

The tumor microenvironment (TME) plays a critical role in NPC progression, with tumor-associated macrophages (TAMs) representing the most abundant immune cell population, comprising 50–80% of non-tumor stromal cells [7,8]. Macrophages exhibit remarkable plasticity and are broadly classified into two polarized phenotypes: classically activated M1 macrophages and alternatively activated M2 macrophages [9,10]. M1 macrophages possess pro-inflammatory and antitumor properties, secreting cytokines such as interleukin-6 (IL-6), interleukin-12 (IL-12), and tumor necrosis factor-α (TNF-α) to promote

* Corresponding author.
E-mail address: zhaoyulinmail@163.com (Y. Zhao).
[1] These authors have contributed equally to this work.

https://doi.org/10.1016/j.tranon.2026.102802
Received 22 February 2026; Received in revised form 8 April 2026; Accepted 27 April 2026

immune responses against cancer cells. Conversely, M2 macrophages exert immunosuppressive and pro-tumorigenic functions through the production of interleukin-10 (IL-10) and transforming growth factor-β (TGF-β), facilitating tumor cell proliferation, angiogenesis, and metastasis [11]. Previous studies have demonstrated that elevated TAM infiltration correlates with poor prognosis and metastatic potential in NPC [12–14]. However, the specific molecular mechanisms by which TAMs, particularly M1 macrophages, contribute to NPC pathogenesis remain largely unexplored [15]. Elucidating the interaction between tumor cells and macrophages, and identifying key regulatory molecules, may provide new insights for NPC diagnosis and treatment [16–19].

In this study, we integrated multiple GEO datasets and employed comprehensive bioinformatics approaches—including CIBERSORT immune infiltration analysis, weighted gene co-expression network analysis (WGCNA), and LASSO regression machine learning—to identify M1 macrophage-associated hub genes in NPC. Among the six hub genes identified, CLIC6 (chloride intracellular channel 6) attracted particular attention due to its consistent downregulation in NPC tissues and significant negative correlation with M1 macrophage infiltration. Subsequent in vitro experiments revealed that CLIC6 expression was significantly reduced in NPC cell lines, and recombinant CLIC6 protein promoted tumor cell proliferation and invasion while suppressing M1 macrophage polarization. Mechanistically, transcriptome sequencing and molecular studies demonstrated that CLIC6 exerts its functions through inhibition of the NF-κB signaling pathway, a master regulator of inflammation and immunity. Functional rescue experiments using NF-κB activator and inhibitor confirmed that CLIC6 regulates NPC cell malignant behaviors and macrophage polarization in an NF-κB-dependent manner. Our findings establish CLIC6 as a novel M1 macrophage-associated tumor suppressor in NPC and reveal a previously unrecognized CLIC6-NF-κB regulatory axis, offering potential therapeutic targets for this challenging malignancy.

Methods

Datasets acquisition and preprocessing

The datasets GSE12452 and GSE53819 were obtained from the Gene Expression Omnibus(GEO, https://www.ncbi.nlm.nih.gov/geo/). GSE12452 comprised 31 NPC samples and 10 normal nasopharyngeal tissues. And GSE53819 consisted of 18 NPC primary tumors and 18 non-cancerous nasopharyngeal tissues. Then we merged the two datasets and removed batch effects with ComBat function from the “sva” R package.

To illustrate the expressions of hub genes, GSE64634 containing 12 NPC and 4 normal nasopharyngeal tissues, was downloaded.

In addition, we used the hub genes to construct logistic equation which classified NPC samples from the GSE102349 into high-and low-risk groups.

Landscape of immune infiltration in NPC

In order to explore immune cells infiltration in NPC, we utilized the CIBERSORTx online platform (https://cibersortx.stanford.edu/) to analyze immune cell infiltration and then visualized the results using the R softwarewith the “ggplot2” package . Between NPC and control group, we compared the relative proportions of 22 immune cells, their intercorrelations were further calculated. Additionally, weighted gene co-expression network analysis (WGCNA) was conducted.

Weighted gene co-expression network analysis (WGCNA)

To investigate the correlations among gene expression and immune cells infiltration in NPC, WGCNA was used to identify highly-correlated gene modules. With the pickSoftThreshold, we set the soft power value ($\beta = 26$) according to the $R2 > 0.9$ criterion. Subsequently, an adjacency matrix was created using a soft power value, which was then converted into a topological overlap matrix (TOM). Subsequently, a hierarchical clustering dendrogram was built so that genes could be divided into distinct modules, using a minimum module size of 30 and a merge cut height of 0.25. Each module’s eigengene (ME) and its correlation with immune cells were calculated, focusing on M1 macrophage-related modules. Significant correlations were found among all genes in the blue module, leading to their selection for further study.

Identification of differentially expressed genes (DEGs)

We obtained the DEGs between NPC samples and control tissues by using “limma” R package in which DEGs qualified for the criteria ($|\log2FC| > 1$, $q < 0.05$). Besides, the heatmap and volcano figures were plotted basing on the “pheatmap” and “ggplot2” R packages. We then identified the intersection of DEGs with the genes in M1 macrophage-associated hub module, labeling them as M1 macrophage-associated DEGs.

Analysis of functional and pathway enrichment

We used the 'Clusterprofiler' R package to perform a Gene Ontology (GO) enrichment analysis, aiming to further explore the biological roles and pathways of DEGs associated with M1 macrophages. The GO annotation included biological process (BP), molecular function(MF) and cellular component (CC) . The most important GO terms was visualized by the “GOplot” R package.

Constructing machine learning model and establishing the risk signature

To further screen the key genes related to M1 macrophages infiltration in NPC, we built the LASSO regression with “glmnet” R packages. In the LASSO regression, we identified the appropriate lambda value using the cv.glmnet function. Then we sorted out those genes based on the criterion that gene-associated coefficient was not equal to zero in the LASSO regression model. Subsequently, logistic regression was performed to acquire the odd ratio (OR), 95% confidence interval of OR, regression coefficients (beta) using the “glm” function. The risk score was computed as follows:

$$Riskscore = \sum_{i=1}^{N}(Coef_i, \times, Exp_i) + 6.76$$

where Expi signifies the expression of genes associated with M1 macrophage,and Coefi is the corresponding regression coefficient. With this regression equation, a risk score was calculated for each tumor sample. We classified the tumor samples into high and low risk groups for the next analysis, basing on the median risk score.

Patient recruitment and clinical specimens

In this study, eleven cases suffering from NPC diseases were enrolled from January 2023 to August 2023. All specimens were pathologically confirmed in accordance with the histological classification criteria for NPC established by the World Health Organization. We also collected 9 control tissues from the noncarcinogenic patients.

RNA extraction and quantitative real-time PCR (qRT-PCT)

Total RNA was extracted from NPC and normal control tissues using Trizol reagent (Invitrogen, USA). The following synthesis of first-strand cDNA was carried out with a reverse transcriptase kit (Vazyme Biotechnology, China). Then we conducted the measurement of mRNA by performing qRT-PCT with SYBR Green PCR Master Mix (Vazyme Biotechnology, China). As an internal control, we selected Glyceraldehyde 3-phosphate dehydrogenase (GAPDH). The mean cycling threshold was determined using the 2 -ΔΔCt method. The primer sequences for the study’ genes were as follows: CLIC6 froward,

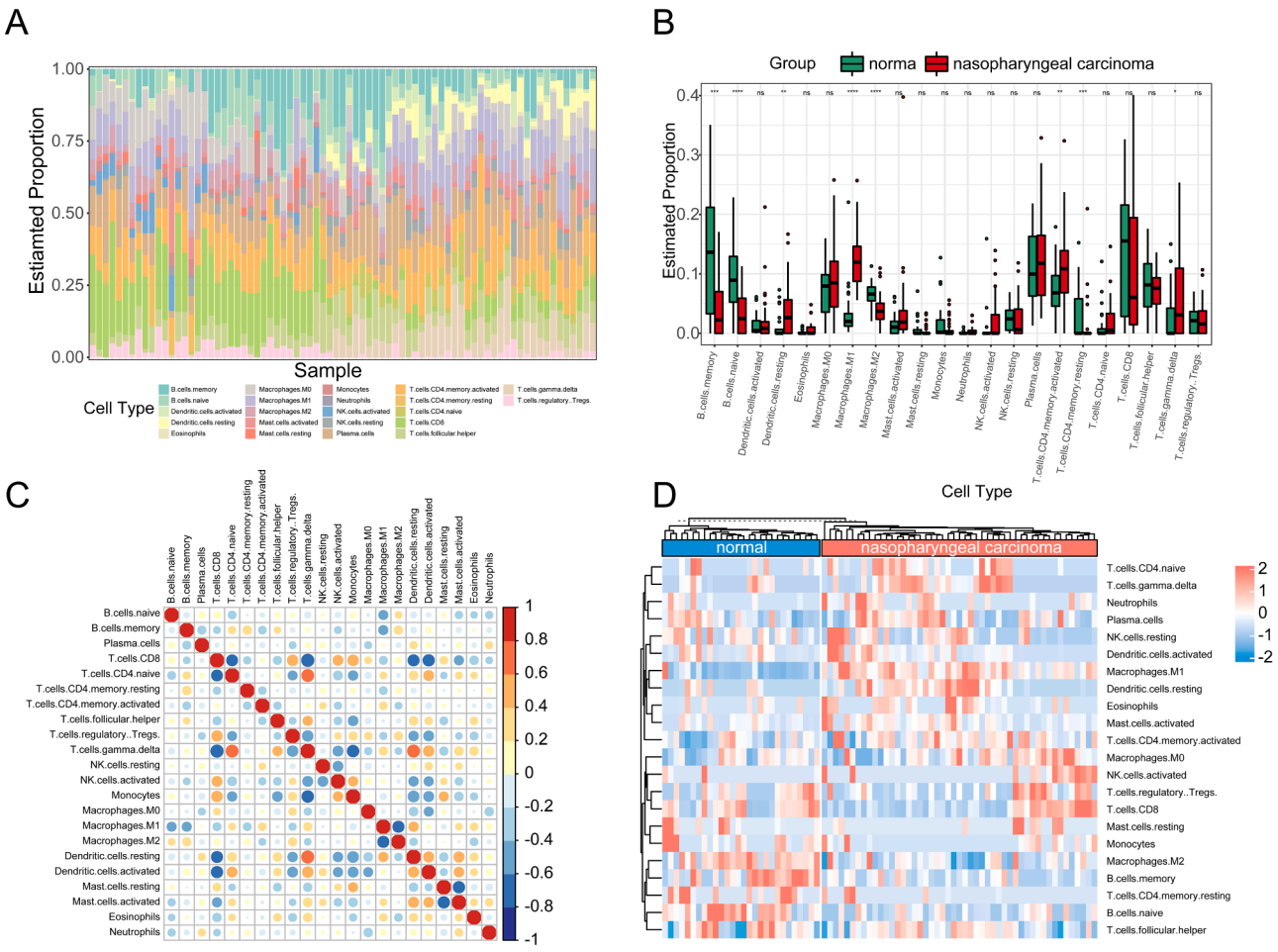

Fig. 1. Immune cells infiltration in NPC and control samples. (A) Estimated percentages of 22 types of immune cells in each sample. (B) Comparison of immune cells infiltration between NPC group and normal group. (C) Correlations among 22 types of infiltrating immune cells (red, positive correlation; blue, negative correlation). (D) Heatmap showing the distributions of 22 kinds of immune cells between the normal and NPC groups. ns: not significant. *P < 0.05, **P < 0.01, ***P < 0.001, ****P < 0.0001.

TCACCCTCTTCGTCAAGGTAA; reverse, AGAGACGCTGAGAAAACGGG. PHYHD1 froward, GAAGTCTGGGCCTCCAGATG; reverse, TTCACCGCCAAAGTGAGGTT. MS4A8 froward, GGGGAGGCTTGTGGTTTATCA; reverse, TTCAAGCCCAAACTGCCAGA. MUC16 froward, CTGGCCA GGGCTGCCT; reverse, CCACGGAGCTGATGAGTGAC. AMIGO1 froward, TCCTCGCCGAGCAGTGAC; reverse, AGGAAGATCTGGGAGGAGGT. MUC20 froward, CAGACGTGAGTGCAGGTGAA; reverse, TCTGGGG TCAGTGAGGTCTT. GAPDH froward, GAAAGCCTGCCGGTGACTAA; reverse, GCCCAATACGACCAAATCAGAG.

Cell lines and culture

Human NPC cell lines (5–8F, HNE-1, and C666–1) and immortalized nasopharyngeal epithelial cell line NP69 were used in this study. 5–8F and HNE-1 cells were cultured in RPMI-1640 medium (Gibco, USA) supplemented with 10% fetal bovine serum (FBS, Gibco). C666–1 cells were maintained in RPMI-1640 medium with 10% FBS. NP69 cells were cultured in keratinocyte serum-free medium (KSFM, Gibco) supplemented with bovine pituitary extract and epidermal growth factor. All cells were incubated at 37 °C in a humidified atmosphere containing 5% CO_2.

Reagents and antibodies

NF-κB activator 1 (HY-12315) and IKK16 (HY-13313) were obtained from MedChemExpress (USA). Antibodies against CLIC6, p65, phospho-p65 (Ser536), IκBα, phospho-IκBα (Ser32/36) were purchased from Proteintech (USA).

Western blot analysis

Cells were lysed in RIPA buffer (Beyotime, China) containing protease and phosphatase inhibitors. Protein concentrations were determined using a BCA protein assay kit (Thermo Fisher Scientific). Equal amounts of protein (30 μg) were separated by SDS-PAGE and transferred onto PVDF membranes (Millipore, USA). Membranes were blocked with 5% non-fat milk in TBST for 1 h at room temperature and incubated overnight at 4 °C with primary antibodies. After washing, membranes were incubated with HRP-conjugated secondary antibodies for 1 h at room temperature. Protein bands were visualized using an ECL chemiluminescence detection kit (Millipore) and imaged with a ChemiDoc XRS+ system (Bio-Rad, USA).

Cell proliferation assay

Cell proliferation was assessed using the Cell Counting Kit-8 (CCK-8, Dojindo, Japan). Cells were seeded in 96-well plates at a density of 3×10^3 cells per well and cultured overnight. After treatment, 10 μL of CCK-8 solution was added to each well and incubated for 2 h at 37 °C. Absorbance was measured at 450 nm using a microplate reader (BioTek, USA). Experiments were performed in triplicate and repeated three times.

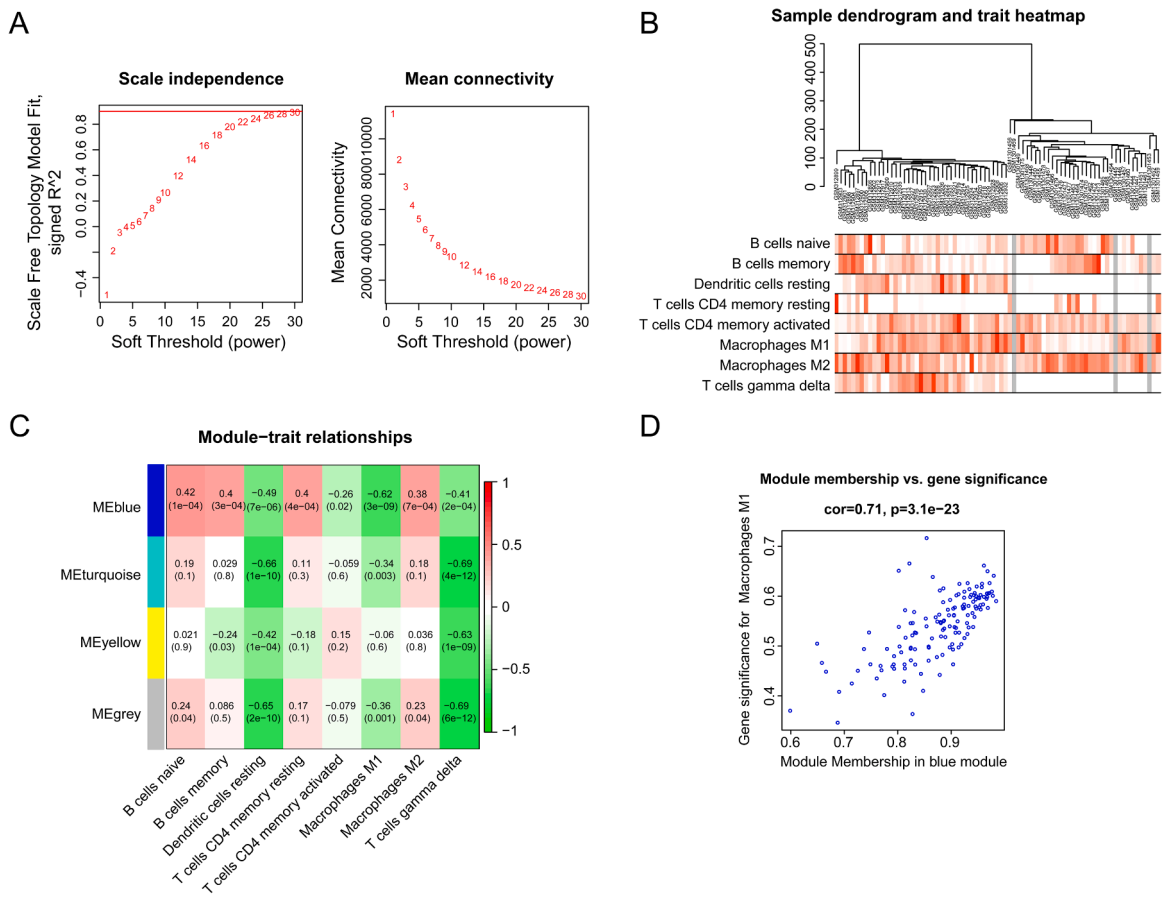

Fig. 2. Construction of weighted co-expression network. (A) Selection of a soft threshold power of 26 (scale-free R2 = 0.9) and establishment of a scale-independent topological network. (B) Hierarchical clustering dendrogram showing clinical grouping features based on color annotations. (C) Correlations between module eigengene and those immune cells which presented significant difference between NPC and control groups. The number in each square indicates correlation coefficients between immune cells infiltration and corresponding modules; meanwhile, P values are shown in the brackets below (red, positive correlation; blue, negative correlation). (D) Correlation of module membership in blue modules and gene significance for M1 macrophages.

Transwell invasion assay

Cell invasion ability was evaluated using Transwell chambers (8 μm pore size, Corning, USA) coated with Matrigel (BD Biosciences, USA). Cells (5×10^4) in 200 μL serum-free medium were seeded into the upper chamber, while 600 μL medium containing 10% FBS was added to the lower chamber as a chemoattractant. After 24 h of incubation, non-invading cells on the upper surface were removed with a cotton swab, and invading cells on the lower surface were fixed with 4% paraformaldehyde and stained with 0.1% crystal violet. Stained cells were counted in five random fields under an inverted microscope (Olympus, Japan).

Macrophage polarization assay

THP-1 cells were induced to M0 macrophages by incubation with 100 ng/mL phorbol 12-myristate 13-acetate (PMA, Sigma, USA) for 48 h. Conditioned medium (CM) from treated NPC cells was collected, centrifuged, and mixed with fresh RPMI-1640 medium at a 1:1 ratio. M0 macrophages were cultured in the CM mixture for 48 h. Total RNA was extracted from macrophages, and expression levels of M1 markers (TNF-α, IL-1β, IL-6) were detected by qRT-PCR.

RNA sequencing and bioinformatics analysis

RNA-seq was performed on HNE-1 cells treated with CLIC6 (500 ng/mL, 24 h; n = 3). Libraries were prepared and sequenced (NovaSeq 6000). Reads were filtered (Fastp), aligned (Hisat2), and quantified (Htseq-Count, FPKM). DEGs were identified by DESeq2 ($|\log_2 FC| > 1$, adj $P < 0.05$). PCA, GO/KEGG, and GSEA analyses were conducted.

siRNA transfection

Three specific siRNAs targeting human CLIC6 (siCLIC6–1, siCLIC6–2, siCLIC6–3) and a negative control siRNA (si-NC) were designed and synthesized by Tsingke Biotechnology (China). The siRNA sequences were as follows: siCLIC6–1 sense: 5′-GGUUAUGAUGGUGAGAGUA-3′, antisense: 5′-UACUCUCACCAUCAUAACC-3′ siCLIC6–2 sense: 5′-GCUAGAGAUGAGUUCACAA-3′, antisense: 5′-UUGUGAACUCAUCUCUAGC-3′ siCLIC6–3 sense: 5′-GAAGCUGGAUAAUUACUUA-3′, antisense: 5′-UAAGUAAUUAUCCAGCUUC-3′ si-NC sense: 5′-UUCUCCGAACGUGUCACGUTT-3′, antisense: 5′-ACGUGACACGUUCGGAGAATT-3′

Cells were seeded in 6-well plates and transfected at 70–80% confluence using Lipofectamine 3000 (Invitrogen, USA) according to the manufacturer's instructions. Briefly, siRNA (50 nM final concentration) and Lipofectamine 3000 were diluted separately in Opti-MEM medium (Gibco), mixed, and incubated for 20 min at room temperature. The mixture was added to cells and incubated for 4–6 h, after which the medium was replaced with fresh complete medium. Transfection efficiency was assessed by qRT-PCR (48 h post-transfection) and Western blot (72 h post-transfection).

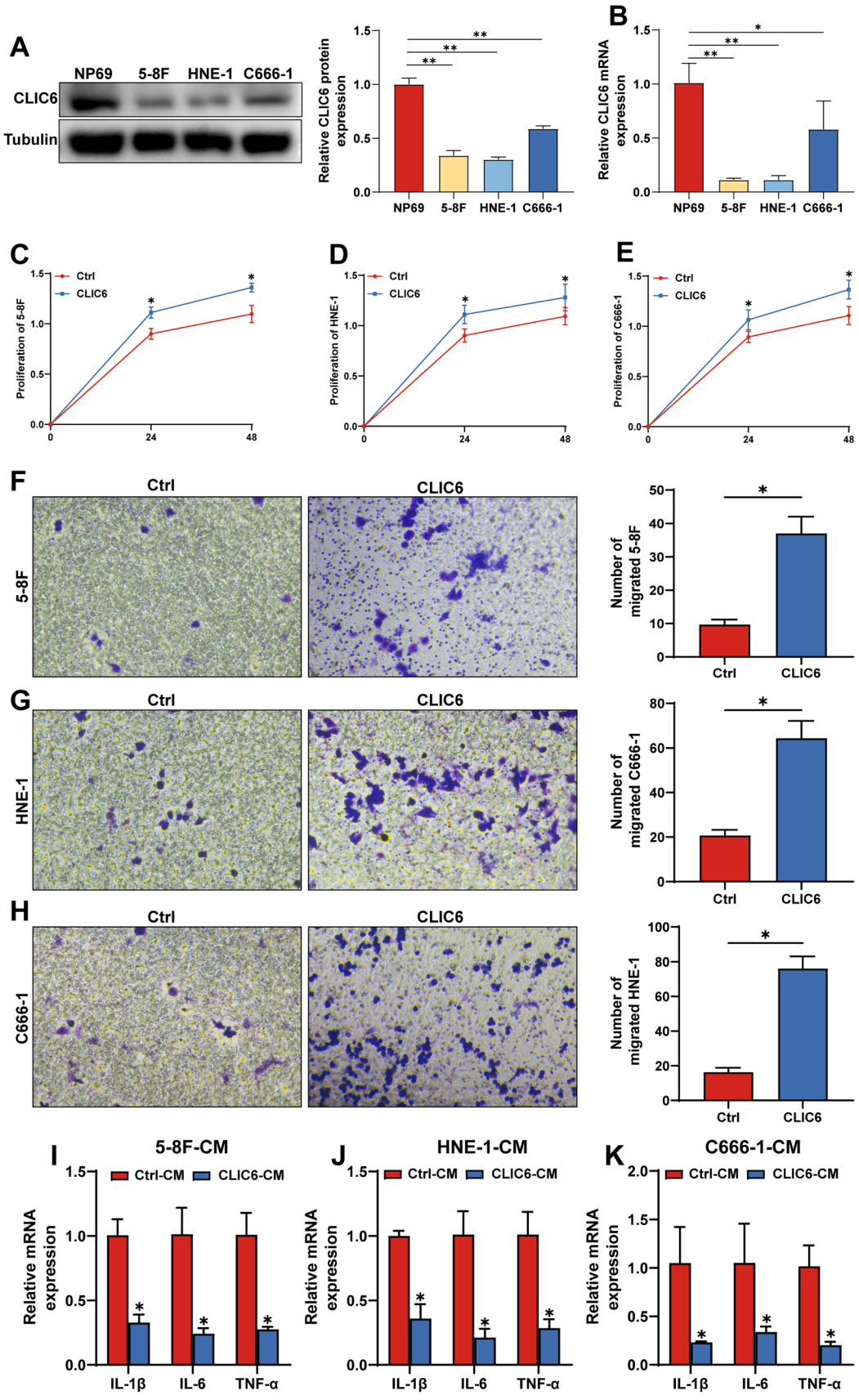

(caption on next page)

Fig. 3. CLIC6 is downregulated in nasopharyngeal carcinoma cell lines and promotes cell proliferation, invasion, and inhibits M1 macrophage polarization. (A) Western Blot detection of CLIC6 protein expression levels in nasopharyngeal carcinoma cell lines (5–8F, HNE-1, C666–1) and human immortalized nasopharyngeal epithelial cells NP69; (B) qRT-PCR detection of CLIC6 mRNA expression levels in the above cells; (C-E) CCK-8 assay for proliferation activity of 5–8F, HNE-1, and C666–1 cells treated with recombinant CLIC6 protein at 24 h and 48 h; (F-H) Transwell assay for changes in invasion capacity of NPC cell lines treated with recombinant CLIC6 protein; (I–K) qRT-PCR analysis of inflammatory marker expression levels (TNF-α, IL-1β, IL-6) in M1 macrophages co-cultured with conditioned medium from CLIC6 recombinant protein-treated NPC cells. *P < 0.05.

Statistical analysis

In this study, R software (Version 4.2.0) was employed for the bioinformatic analysis. The qPCR experiment was repeated for three times to measure the mRNA expression of hub genes. Data were expressed as mean ± standard deviation, and an unpaired Student's *t*-test was utilized for analysis. Pearson correlation was applied to analyze the correlation. All figures were typeset by Adobe Illustration CC 2018. P values < 0.05 were considered statistically significant.

Results

Brief recapitulation of study design

The flowchart was presented in Supplementary Figure 1. At first, GSE12452 and GSE53819 containing NPC samples from GEO were merged. We conducted the CIBERSORT and WGCNA algorithm to confirm the hub gene module related to M1 macrophages in NPC samples. Next, we identified the M1 macrophage-associated hub genes by taking the intersection of DEGs and genes in hub module. To further pinpoint the hub genes in the process of M1 macrophage filtration, we built the machine learning model and acquired 6 hub genes including MUC16, MS4A8, MUC20, AMIGO1, PHYHD1 and CLIC6. Finally, we verified the mRNA expressions of these hub genes in NPC and control mucous samples by RT-qPCR method. In addition, we used logistic regression to divide GSE102349 dataset into high- and low- risk groups, and analyzed the stromal and immune scores between the two groups.

We merged GSE12452 and GSE53819, and drew a box diagram to show the distribution of gene expressions in the samples (Supplementary Figure 2A). Then we applied principal component analysis (PCA) with "FactoMineR" and "factoextra" R packages to examine the merged data (Supplementary Figure 2B), which displayed the batch effects between the two datasets. Then, ComBat function in "sva" R package was applied to remove batch effects (Supplementary Figure 2C). As illustrated in Supplementary Figure 2D, the scatter points on behalf of the samples within the group showed mutual aggregation, indicating a better repeatability of data.

Analysis of immune cell filtration in NPC sample

Emerging evidences has revealed the key function of infiltrated immune cells in tumor development and prognosis, but whether immune infiltration contributed to the process of NPC deserved to be explored. Herein, we employed CIBERSORT algorithm to analyze the relative abundance of 22 types immune cells in NPC and normal tissues. The histogram in Fig. 1A displayed the estimated percentages of immune cells in each sample. In Fig. 1B, we further showed that the proportions of M1 macrophages, resting dendrite cells, activated CD4 memory T cells and gamma delta T cells in NPC samples were significantly increased, while M2 macrophages, memory B cells, naive B cells, and resting CD4 memory T cells were decreased when comparing with healthy tissues. Next, we investigated the correlations of different types of immune cells. The results exhibited M1 macrophages had significantly positive correlations with activated CD4 memory T cells, gamma delta T cells and resting dendritic cells, but inversely presented negative correlations with M2 macrophages, memory B cells, naive B cells, and resting CD4 memory T cells (Fig. 1C). The heatmap showed the distributions of 22 kinds of immune cells between the normal and NPC groups (Fig. 1D). Therefore, we proposed that M1 macrophages might play a fundamental role in the pathological mechanism of NPC disease.

Development of a co-expression network and detection of hub modules related to M1 macrophages

To identify the genes related to M1 macrophage in NPC subjects, we employed WGCNA and divided the genes into different modules. The "pickSoftThreshold" function was used to automatically select a soft threshold power of 26 (scale-free R2 = 0.9) and Fig. 2A also showed the mean connectivity in different soft thresholds. Next, the plotDendroAndColors function was used to plot hierarchical clustering dendrogram (Fig. 2B). The data was clustered into 4 modules based on hierarchical clustering method and these modules were marked with different colors. We calculated the correlations between different gene modules and immune cells using Pearson correlation analysis. The results indicated the blue module had a significantly negative correlation with M1 macrophage filtration (r = −0.62, p = 3e-09), as shown in Fig. 2C. The membership in blue module and gene significance for M1 macrophage had a marked correlation as illustrated in Fig. 2D (r = 0.71, p = 3.1e-23). Finally, we identified the blue module including 143 genes as the hub one which was highly correlated to M1 macrophage infiltration in NPC subjects, and these genes were selected for subsequent analysis.

Identification of M1 macrophage-associated DEGs

In order to further identify the genes associated with M1 macrophage infiltration in NPC, we screened out the DEGs and took the overlap of the DEGs and the blue module mentioned above. The volcano plot in Supplementary Figure 3A demonstrated that A total of 828 DEGs were identified in NPC samples, comprising 301 up-regulated and 527 down-regulated genes. We obtained 131 DEGs as the M1 macrophage-associated hub genes by intersecting the 828 DEGs and the genes in blue module (Supplementary Figure 3B). Supplementary Figure 3C illustrates the relative expression levels of genes associated with M1 macrophages. These genes were utilized for further functional enrichment analysis.

Function enrichment and biological pathway in M1 macrophage-associated DEGs

To investigate the biological function and potential signaling pathway of M1 macrophage-associated DEGs, GO enrichment analysis was performed. The BP terms with the highest enrichment included microtubule-based movement, cilium movement, cilium organization, cilium assembly, and cell motility dependent on cilia or flagella (Supplementary Figure 4A). The most enriched MF terms were tubulin binding, cytoskeletal motor activity, microtubule motor activity and microtubule binding (Supplementary Figure 4B). The most enriched CC terms were motile cilium, axoneme, ciliary plasm and plasm membrane bounded cell projection cytoplasm (Supplementary Figure 4C). The GO analysis findings showed that DEGs linked to M1 macrophages were primarily associated with cilium movement based on microtubules and tubulin binding. A chord graph was used to visualize the most enriched GO terms and associated genes (Supplementary Figure 4D) and in a cluster graph (Supplementary Figure 4E). Hence, we made a conjecture that M1 macrophage-associated immune response might damage the

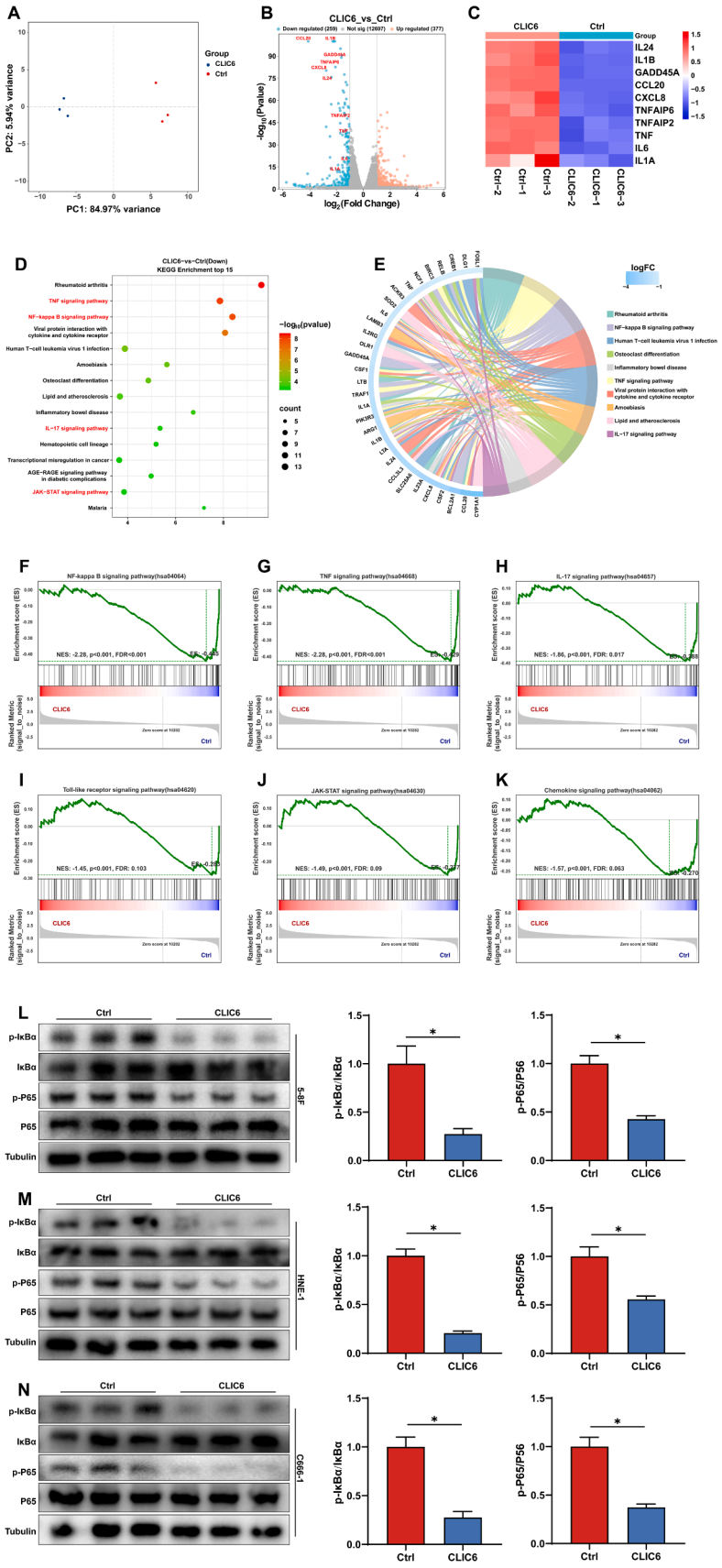

(caption on next page)

Fig. 4. CLIC6 recombinant protein treatment induces transcriptional reprogramming in HNE-1 cells, significantly suppressing inflammatory gene expression and signaling pathways, with validation of its inhibitory effect on the NF-κB pathway at the protein level. (A) Principal Component Analysis (PCA) reveals overall transcriptional differences between CLIC6 recombinant protein-treated and control HNE-1 cells; (B) Heatmap clustering analysis reveals the downregulated inflammatory gene expression profile in the CLIC6-treated group; (C) Expression level comparison of representative inflammatory genes (CCL20, CXCL8, IL1B, IL6, IL1A, IL24, TNF, GADD45A, TNFAIP6, TNFAIP2) in the CLIC6-treated group; (D) KEGG pathway enrichment analysis bubble chart showing significantly downregulated inflammation-related signaling pathways in the CLIC6-treated group; (E) Gene-pathway association network diagram (cnetplot) illustrating the relationship between downregulated genes and inflammatory pathways; (F-K) Gene Set Enrichment Analysis (GSEA) validating the inhibitory effects of CLIC6 treatment on the NF-κB signaling pathway, TNF signaling pathway, IL-17 signaling pathway, Toll-like receptor signaling pathway, JAK-STAT signaling pathway, and chemokine signaling pathway; (L-N) Western Blot analysis of changes in phosphorylation levels of core NF-κB signaling molecules IκBα and P65 in 5–8F, HNE-1, and C666–1 cells following CLIC6 recombinant protein treatment. *P < 0.05, **P < 0.01.

cilium movement and assembly of the epithelial cells in the nasopharynx in NPC.

Machine learning model and validation in GEO dataset

To further pinpoint M1 macrophage-associated DEGs in NPC, 131 DEGs were used to construct machine learning model like LASSO regression model. We used the "glmnet" package to carry out lambda. min and lambda.1se (Supplementary Figure 5A). Lambda.1se was selected to calculate the coefficient of each gene by using the coef function. And those genes whose coefficients were not equal to 0 were reserved (Supplementary Figure 5B). Eventually, we identified six M1 macrophage-associated genes, such as CLIC6, PHYHD1, MS4A8, MUC16, AMIGO1 and MUC20. These genes were validated in the GSE64634 (Supplementary Figure 5C). And we found these six genes presented significantly lower expressions in NPC group. Next, we employed the six hub genes to create a logistic regression model for prediction. Among these genes, MUC16, MUC20, AMIGO1, PHYHD1, and CLIC6 had a negative effect on nasopharyngeal carcinogenesis with odd ratios (ORs) < 1 except for OR value of MS4A8 > 1(Supplementary Figure 5D). These results reminded us that MUC16, MUC20, AMIGO1, PHYHD1, and CLIC6 might exert a negative regulation of the pathological process of NPC disease.

Verification of M1 macrophage-related hub genes in NPC and control samples

Using the RT-qPCR method, we confirmed the reliability of the six hub genes by detecting mRNA expression levels in nasal tissues from 11 patients with NPC and 9 control subjects. In Supplementary Figure 6, the results presented decreased mRNA expressions of MUC16, MUC20, AMIGO1, PHYHD1, and CLIC6 in NPC samples, through MUC20 did not have a statistical difference due to a small sample size or NPC pathological subtypes probably. The low expressions of six hub genes in NPC subjects were consistent with the above results, which indicated these genes might interact with M1 macrophages to facilitate the progression of NPC.

Establishing the M1 macrophage-related risk signature

Six M1-related genes were used to construct a risk model in GSE102349. High-risk patients showed upregulation of cancer-immunity cycle inhibitors and immune checkpoints (Supplementary Figure 7A–B), along with decreased immune/stromal scores (Supplementary Figure 7C). Correlation analysis linked these genes to immunosuppressive markers (Supplementary Figure 7D–E). Low expression of key genes, including CLIC6, predicted immunosuppression and poor prognosis.

Analysis of immune cells infiltration between NPC low- and high-risk groups

CIBERSORT revealed immune cell distributions (Supplementary Figure 8A–B) and correlations (Supplementary Figure 8C). M1 macrophages negatively correlated with B cells, M2 macrophages, and CD4 memory T cells, but weakly positively with dendritic cells. Hub genes, including CLIC6 and AMIGO1, were negatively associated with M1 macrophages (Supplementary Figure 8D), supporting model validity.

CLIC6 is downregulated in nasopharyngeal carcinoma cells, and its recombinant protein promotes malignant phenotypes in tumor cells while inhibiting M1 macrophage polarization

To validate the bioinformatics analysis finding that CLIC6 is downregulated in nasopharyngeal carcinoma (NPC), we first assessed its expression levels in NPC cell lines. Western Blot (Fig. 3A) and qRT-PCR (Fig. 3B) results both showed that compared to the immortalized nasopharyngeal epithelial cell line NP69, CLIC6 mRNA and protein expression levels were significantly downregulated (P < 0.05) in the three NPC cell lines 5–8F, HNE-1, and C666–1, confirming the bioinformatics analysis results.

Given its low expression profile, we further investigated the impact of CLIC6 on NPC cell biological behaviors. CCK-8 proliferation assays (Fig. 3C-E) and Transwell invasion assays (Fig. 3F-H) demonstrated that exogenous CLIC6 recombinant protein treatment significantly enhanced the proliferation and invasive capabilities of all three NPC cell lines (P < 0.05). Furthermore, based on the bioinformatics analysis revealing a negative correlation between CLIC6 and M1-type macrophages, conditioned medium from NPC cells treated with CLIC6 recombinant protein was collected and co-cultured with M0-type macrophages. qRT-PCR detection revealed that this conditioned medium significantly suppressed the expression of M1 macrophage markers TNF-α, IL-1β, and IL-6 (P < 0.05, Fig. 3I-K). These results indicate that CLIC6 not only directly promotes the malignant phenotype of NPC cells but may also suppress anti-tumor immunity by reshaping the tumor microenvironment.

CLIC6 reshapes the NPC transcriptome landscape, primarily suppressing the NF-κB inflammatory signaling pathway

RNA-seq of HNE-1 cells showed CLIC6 markedly altered gene expression (Fig. 4A–C), with downregulation of inflammatory genes (e.g., CCL20, CXCL8, IL1B, TNF). KEGG and GSEA revealed suppression of NF-κB, TNF, and IL-17 pathways, with NF-κB most significantly inhibited (Fig. 4D–K). Western blot confirmed reduced phosphorylation of IκBα and p65 without affecting total levels (Fig. 4L–N), indicating inhibition at transcriptional and protein levels.

CLIC6 regulates NPC cell proliferation, invasion, and macrophage polarization by inhibiting the NF-κB signaling pathway

To further determine whether CLIC6′s regulation of NPC malignant phenotypes depends on the NF-κB signaling pathway, we performed functional rescue experiments. Following treatment with CLIC6 recombinant protein, we co-administered an NF-κB pathway activator (NF-κB activator 1). Western blot results showed that this activator effectively reversed CLIC6′s inhibition of IκBα and p65 phosphorylation (Fig. 5A-C).

Correspondingly, at the cellular functional level, the NF-κB activator significantly attenuated the CLIC6-promoted proliferation (Fig. 5D-F) and invasion (Fig. 5G-I) effects. Furthermore, in macrophage co-culture

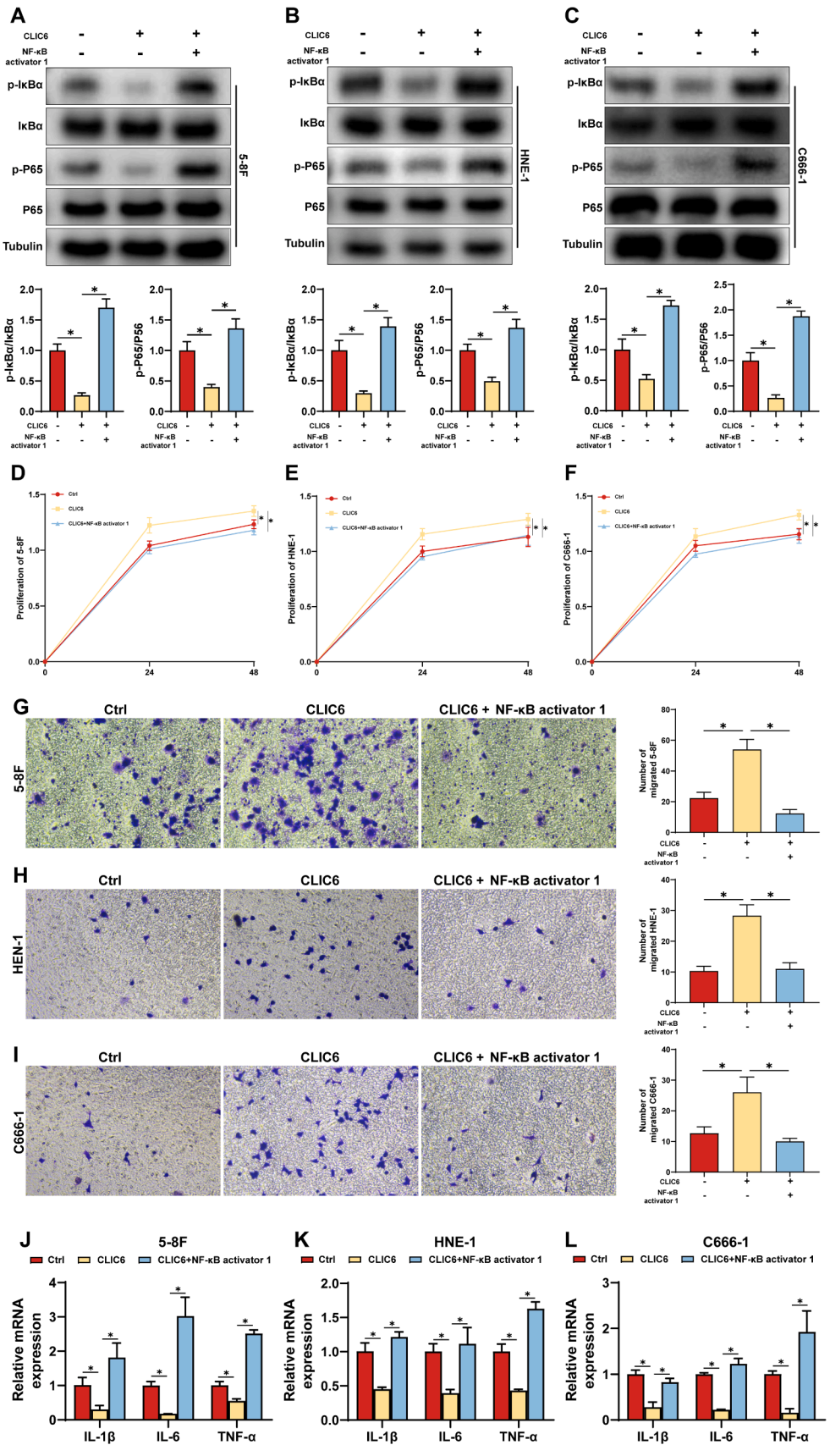

(caption on next page)

Fig. 5. NF-κB pathway activators reverse the regulatory effects of CLIC6 on malignant biological behavior in nasopharyngeal carcinoma cells and macrophage polarization. (A–C) Western Blot analysis of changes in IκBα and P65 protein phosphorylation levels in 5–8F, HNE-1, and C666–1 cells following co-treatment with NF-κB activator 1 and CLIC6 recombinant protein; (D–F) CCK-8 assay measuring proliferation activity of NPC cell lines under the aforementioned treatment conditions; (G-I) Transwell assay showing changes in invasion capacity of NPC cell lines under the aforementioned treatment conditions; (J-L) qRT-PCR detecting expression levels of M1 macrophage inflammatory markers TNF-α, IL-1β, and IL-6 after co-culture with conditioned medium from NPC cells in each treatment group. *P < 0.05, **P < 0.01.

systems, the NF-κB activator similarly reversed CLIC6′s suppression of M1 macrophage polarization, manifested as restored expression of proinflammatory factors (TNF-α, IL-1β, IL-6) (Fig. 5J-L). These findings confirm that CLIC6 exerts its dual functions of promoting NPC malignant progression and suppressing antitumor immunity by inhibiting the NF-κB signaling pathway.

Silencing CLIC6 activates the nf-κb pathway, suppresses the malignant phenotype of NPC, and promotes M1 macrophage polarization

To reverse-validate CLIC6′s function, we employed siRNA technology to knockdown CLIC6 expression in three NPC cell lines (Fig. 6A-F). Results showed that CLIC6 silencing significantly increased IκBα and p65 phosphorylation levels, activating the NF-κB signaling pathway—an effect blocked by the NF-κB-specific inhibitor IKK16 (Fig. 6G-I).

Functionally, CLIC6 silencing markedly suppressed NPC cell proliferation (Fig. 6J-L) and invasion capacity (Fig. 6M-O), while co-treatment with IKK16 partially reversed these inhibitory effects. Finally, in a macrophage co-culture system, conditioned medium from CLIC6-silenced NPC cells significantly promoted M1 macrophage polarization, an effect similarly antagonized by IKK16 (Fig. 6P-R). These results provide further evidence from a reverse genetics perspective that CLIC6 regulates NPC cell function and tumor-associated macrophage polarization by inhibiting the NF-κB signaling pathway.

Discussion

Nasopharyngeal carcinoma (NPC) is a distinct head and neck malignancy with unique epidemiological and etiological characteristics, closely associated with Epstein-Barr virus (EBV) infection, genetic susceptibility, and environmental factors [20–22]. Despite advances in radiotherapy and chemotherapy, patients with recurrent or metastatic disease still face poor prognosis, underscoring the urgent need for novel therapeutic targets [23,24]. The tumor microenvironment (TME), particularly tumor-associated macrophages (TAMs), plays a pivotal role in NPC progression and therapeutic response [25]. However, the molecular mechanisms linking TAMs to NPC pathogenesis remain incompletely understood [26]. In this study, we integrated bioinformatics analysis with in vitro experiments to systematically investigate the role of CLIC6, an M1 macrophage-associated hub gene, in NPC.

Through comprehensive bioinformatics analysis of GEO datasets, we first identified that M1 macrophages were significantly enriched in NPC tissues compared to normal controls, while M2 macrophages showed decreased infiltration. Our WGCNA analysis identified a blue module significantly negatively correlated with M1 macrophage infiltration, and functional enrichment analysis revealed that genes in this module were primarily associated with cilium assembly and movement. This intriguing finding suggests that M1 macrophage-associated immune responses might compromise ciliary function in nasopharyngeal epithelial cells, potentially contributing to NPC pathogenesis [13,14].

By intersecting DEGs with the blue module genes and applying LASSO regression, we identified six M1 macrophage-associated hub genes: CLIC6, PHYHD1, MS4A8, MUC16, AMIGO1, and MUC20. Among these, CLIC6 particularly captured our attention due to its consistent downregulation across multiple datasets and its significant negative correlation with M1 macrophages. Chloride intracellular channel 6 (CLIC6) belongs to the CLIC family of metamorphic proteins that exist in both soluble and membrane-associated forms, participating in diverse cellular processes including cell cycle regulation, apoptosis, and metastasis [27,28]. While CLIC family members have been implicated in various cancers—for instance, CLIC1 promotes gastric cancer progression and CLIC4 exhibits tumor-suppressive functions in certain contexts—the role of CLIC6 in NPC has not been previously characterized [29–31]. Our RT-qPCR validation in clinical specimens confirmed significantly lower CLIC6 expression in NPC tissues compared to normal controls, consistent with our bioinformatics predictions and suggesting a potential tumor-suppressive role. CLIC6 promotes NPC proliferation and invasion while suppressing NF-κB signaling, evidenced by reduced IκBα and p65 phosphorylation, suggesting a compensatory mechanism despite its low tumor expression. The NF-κB pathway holds particular significance in NPC pathogenesis [32]. While NF-κB activation is traditionally associated with promoting inflammation and tumor progression, its role in cancer is context-dependent and can even be tumor-suppressive under certain conditions [33,34]. Our findings reveal that CLIC6-mediated NF-κB inhibition actually promotes NPC cell proliferation and invasion, suggesting that in the NPC context, basal NF-κB activity might exert tumor-suppressive effects—a notion supported by some recent studies showing that excessive NF-κB activation can trigger senescence and apoptosis [35–38]. The functional rescue experiments using NF-κB activator 1 provided definitive evidence: restoration of NF-κB signaling significantly attenuated CLIC6-induced proliferation and invasion, establishing a causal relationship. CLIC6 modulates the immune microenvironment via NF-κB–dependent regulation of NPC secretory profiles, suppressing M1 macrophage polarization and promoting immunosuppression. A six-gene risk model links low CLIC6 expression to immune-inhibitory features and poor prognosis. Limitations include small sample size, lack of in vivo validation, and unclear mechanisms underlying NF-κB regulation.

Conclusions

This study integrates bioinformatics analysis with experimental validation to establish CLIC6 as a novel M1 macrophage-associated tumor suppressor in NPC. We demonstrate that CLIC6 inhibits NPC cell proliferation, invasion, and modulates macrophage polarization through suppression of NF-κB signaling. The identification of a CLIC6-centered regulatory axis linking intrinsic tumor properties with immune microenvironment offers new insights into NPC pathogenesis and suggests that restoring CLIC6 function or targeting its downstream effectors might represent therapeutic opportunities. Future studies should focus on elucidating the structural basis of CLIC6-mediated NF-κB regulation, validating its therapeutic potential in preclinical models, and exploring its value as a biomarker for patient stratification and prognosis prediction in NPC.

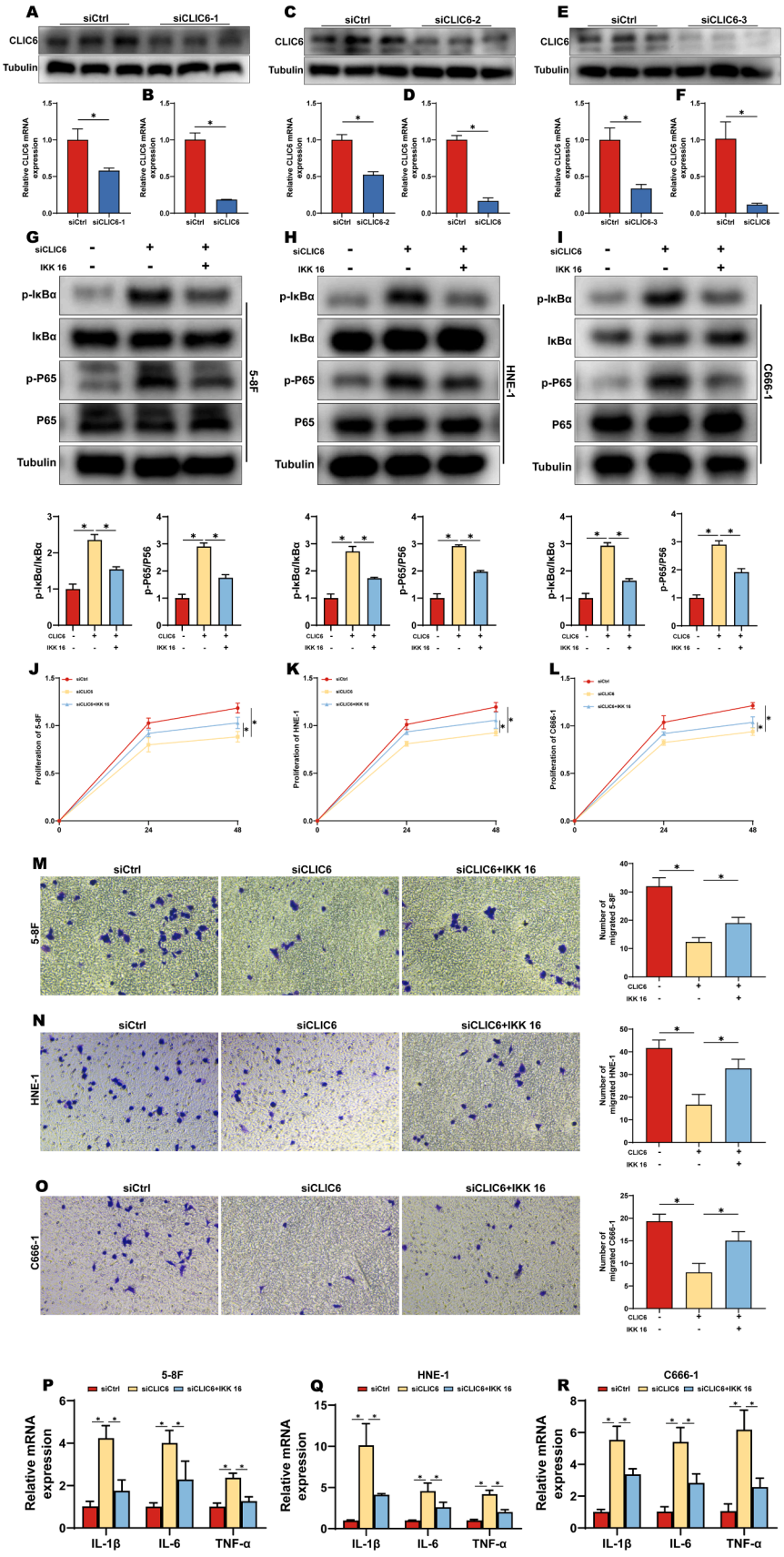

(caption on next page)

Fig. 6. siRNA-mediated CLIC6 gene silencing activates the NF-κB signaling pathway and suppresses the malignant phenotype of nasopharyngeal carcinoma cells, while IKK16 partially reverses this effect. (A-C) qRT-PCR detection of CLIC6 mRNA expression levels in three nasopharyngeal carcinoma cell lines (5–8F, HNE-1, C666–1) after transfection with three CLIC6-specific siRNAs and the negative control siRNA-NC; (D-F) Western Blot analysis of CLIC6 protein expression levels post-transfection; siRNA-3, exhibiting the highest silencing efficiency, was selected for subsequent experiments; (G-I) Western Blot analysis of changes in IκBα and P65 protein phosphorylation levels in each nasopharyngeal carcinoma cell line following treatment with siCLIC6 alone or in combination with the NF-κB pathway inhibitor IKK16; (J-L) CCK-8 assay to detect proliferation activity in each cell line after the above treatments; (M-O) Transwell assay to detect changes in invasion capacity in each cell line after the above treatments; (P-R) qRT-PCR to detect expression levels of M1 macrophage inflammatory markers TNF-α, IL-1β, and IL-6 after co-culture with conditioned medium from NPC cells in each treatment group. *P < 0.05, **P < 0.01.

Ethics statement and consent to participate

The studies involving human participants were reviewed and approved by Ethical Committee of the first affiliated Hospital of Zhengzhou University School(No.2021-KY-1024–002), in compliance with the guidelines outlined in the Declaration of Helsinki. The patients/participants provided their written informed consent to participate in this study.

Funding

This study was supported by grants from Henan Medical Researcher Overseas Training Program (HNMOT2024060), General Program of National Natural Science Foundation of China (82071023) and Joint Construction Project of Medical Science and Technology of Henan Province (LHGJ20190194).

Publisher's note

All claims expressed in this article are solely those of the authors and do not necessarily represent those of their affiliated organizations, or those of the publisher, the editors and the reviewers. Any product that may be evaluated in this article, or claim that may be made by its manufacturer, is not guaranteed or endorsed by the publisher.

Data availability statement

The datasets presented in this study can be found in online repositories. The names of the repository/repositories and accession number(s) can be found below: https://www.ncbi.nlm.nih.gov/geo/ (GSE12452, GSE53819, GSE64634 and GSE102349).

CRediT authorship contribution statement

Zhuo Chen: Writing – original draft, Supervision, Resources, Methodology, Funding acquisition, Formal analysis, Data curation. **Mingxian Li:** Writing – original draft, Validation, Software, Project administration, Methodology, Investigation. **Pei Gao:** Software, Resources, Project administration, Methodology. **Yulin Zhao:** Writing – review & editing, Visualization, Funding acquisition, Conceptualization.

Declaration of competing interest

The authors declare no competing interest.

Acknowledgments

We thank the researchers who contributed to the GEO datasets, as well as the patients and healthy volunteers who participated in this study.

Supplementary materials

Supplementary material associated with this article can be found, in the online version, at doi:10.1016/j.tranon.2026.102802.

References

[1] R. He, P. Jie, Z. Wang, Y. Lu, H. Lv, Z. Huang, et al., Artificial intelligence-assisted real-time nasopharyngeal cancer diagnostic model enhances rhinologist performance: a prospective multi-reader study, Ann. Med. 58 (2026) 2620335.
[2] Z.-Y. Zhao, S.-Q. He, G.-Y. Liu, S.-H. Lv, Y.-H. Yu, G.-Y. Zhang, et al., Efficacy of radiotherapy to metastatic lesion in de novo metastatic nasopharyngeal carcinoma patients: a multicenter, propensity score matching study, Oral Oncol. 175 (2026) 107907.
[3] Y. Yang, C.-J. Yen, J. Pan, H. Wang, S. Qu, N. Chen, et al., First-line Tislelizumab plus chemotherapy for recurrent or metastatic nasopharyngeal cancer: three-year follow-up of the phase 3 RATIONALE-309 randomized clinical trial, JAMa Oncol. 12 (2026) 384, https://doi.org/10.1001/jamaoncol.2026.0020.
[4] Y. Huang, D. Sun, H. Zhou, T. Zhou, S. Qu, J. Li, et al., Five-year outcome of Camrelizumab Plus chemotherapy in recurrent or metastatic nasopharyngeal carcinoma: a secondary analysis of the CAPTAIN-1st randomized clinical trial, JAMa Oncol. (2026) e256245.
[5] C. Wang, Y. Xiao, L. Wu, Y. He, M. Chen, W. Hu, et al., Humanistic nursing care and quality of life in patients with nasopharyngeal carcinoma: a prospective observational study, BMC. Nurs. 25 (2026) 304, https://doi.org/10.1186/s12912-026-04455-9.
[6] K. Stawarz, A. Gorzelnik, W. Klos, J. Korzon, F. Kissin, K. Bienkowska-Pluta, et al., Immunotherapy for locoregionally advanced nasopharyngeal carcinoma: a meta-analysis of randomized clinical trials, Ther. Adv. Med. Oncol. 18 (2026) 17588359251412043.
[7] B. Zhang, T. Miao, X. Shen, L. Bao, C. Zhang, C. Yan, et al., EB virus-induced ATR activation accelerates nasopharyngeal carcinoma growth via M2-type macrophages polarization, Cell Death. Dis. 11 (2020) 742.
[8] F. Luo, J. Cao, Q. Chen, L. Liu, T. Yang, X. Bai, et al., HDL-cholesterol confers sensitivity of immunotherapy in nasopharyngeal carcinoma via remodeling tumor-associated macrophages towards the M1 phenotype, J. ImmunOther Cancer 12 (2024) e008146.
[9] W. Chen, L. Bao, Q. Ren, Z. Zhang, L. Yi, W. Lei, et al., SCARB1 in extracellular vesicles promotes NPC metastasis by co-regulating M1 and M2 macrophage function, Cell Death. Discov. 9 (2023) 323.
[10] Z. Huang, Y. Li, Q. Liu, X. Chen, W. Lin, W. Wu, et al., SPP1-mediated M2 macrophage polarization shapes the tumor microenvironment and enhances prognosis and immunotherapy guidance in nasopharyngeal carcinoma, Int. Immunopharmacol. 147 (2025) 113944.
[11] C. Huang, X. Wang, L. Wang, Y. Liu, Z. Xia, X. Wang, et al., Targeting tumor associated macrophages (TAMs) reprograms tumor immune microenvironment to promote solid tumor immunotherapy, Cell Oncol. (Dordr) 47 (2024) 2011–2014.
[12] F. Luo, H. Li, W. Ma, J. Cao, Q. Chen, F. Lu, et al., The BCL-2 inhibitor APG-2575 resets tumor-associated macrophages toward the M1 phenotype, promoting a favorable response to anti-PD-1 therapy via NLRP3 activation, Cell Mol. Immunol. 21 (2024) 60–79.
[13] Y. Yu, L. Ke, X. Lv, Y.H. Ling, J. Lu, H. Liang, et al., The prognostic significance of carcinoma-associated fibroblasts and tumor-associated macrophages in nasopharyngeal carcinoma, Cancer Manage Res. 10 (2018) 1935–1946.
[14] J.-W. Chen, R.-N. Shen, J.-Q. Zhu, Y.-H. Wang, L-M. Fu, Y.-H. Chen, et al., Transcriptomic profiling reveals mechanism, therapeutic potential, and prognostic value of cancer stemness characteristic in nasopharyngeal carcinoma, Funct. Integr. Genomics. 25 (2025) 56.
[15] Q. Liu, T. Yang, Y. Zhang, Z.-D. Hu, Y.-M. Liu, Y.-L. Luo, et al., ZIC2 induces pro-tumor macrophage polarization in nasopharyngeal carcinoma by activating the JUNB/MCSF axis, Cell Death. Dis. 14 (2023) 455.
[16] X. Zhang, S. Qian, P. Wu, B. Yu, D. Yin, X. Peng, et al., Tumor-associated macrophage-derived itaconic acid contributes to nasopharyngeal carcinoma progression by promoting immune escape via TET2, Cell Commun. Signal. 22 (2024) 413.
[17] Y. Wu, R. Sun, S. Ren, G. Zengin, M. Li, Neuronal reshaping of the tumor microenvironment in tumorigenesis and metastasis: bench to clinic, Med. Adv. 3 (2025) 364–371.
[18] M.-Y. Li, Q. Zhang, G. Zengin, Q. Guo, W. Sun, Spatial omics: deciphering heterogeneity in the tumor immune microenvironment and resistance to immunotherapy, Curr. Proteomics. 22 (2025) 100055.
[19] Y. Wu, R. Sun, G. Zengin, S. Ren, Li M-Y.Tumor Organoids, Breakthroughs in clinical decision making, drug development, and translational advances beyond conventional models, Med. Res. 2 (2026) 26–40, https://doi.org/10.1002/mdr2.70048, n/a.
[20] J. Zhou, Y. Hua, C. Zhang, Q. Liu, Y. Deng, Y. Kuang, et al., Multimodal glyco-lipid-EBVDNA signature prognostic model for individualized risk stratification of locally advanced nasopharyngeal carcinoma, Eur. J. Nucl. Med. Mol. ImAging (2026), https://doi.org/10.1007/s00259-026-07781-x.

[21] N. Liu, B. Meng, Y. Li, M. Tang, Y. Cao, L. Shang, et al., Nasopharyngeal carcinoma at the Virology Precision Oncology Nexus: decoding molecular alterations for early intervention and therapeutic innovation, Biomolecules. 16 (2026) 256.
[22] J. Li, W. Cai, Q. Wu, C. Tang, Y. Cao, Y. Song, Network analysis of symptom clusters and core symptom changes in nasopharyngeal cancer survivors: a longitudinal study, J. Cancer Surviv. (2026), https://doi.org/10.1007/s11764-026-01987-6.
[23] R. You, G.-Q. Xu, X. Ding, J.-H. Liang, Z.-G. Liu, X. Zou, et al., Standard chemoradiotherapy with concurrent and adjuvant camrelizumab in patients with high risk nasopharyngeal carcinoma: multicentre, randomised, open label, phase 3 trial, BMJ 392 (2026) e085863.
[24] The Lancet Regional Health-Americas null. Nonmetastatic nasopharyngeal carcinoma: in search of safer therapies, Lancet Reg. Health Am. 54 (2026) 101420.
[25] P. Chen, D. Wang, T. Xiao, W. Gu, H. Yang, M. Yang, et al., ACSL4 promotes ferroptosis and M1 macrophage polarization to regulate the tumorigenesis of nasopharyngeal carcinoma, Int. Immunopharmacol. 122 (2023) 110629.
[26] W.-S. Peng, X. Zhou, W.-B. Yan, Y.-J. Li, C.-R. Du, X.-S. Wang, et al., Dissecting the heterogeneity of the microenvironment in primary and recurrent nasopharyngeal carcinomas using single-cell RNA sequencing, Oncoimmunology. 11 (2022) 2026583.
[27] V. Loyo-Celis, D. Patel, S. Sanghvi, K. Kaur, D. Ponnalagu, Y. Zheng, et al., Biophysical characterization of chloride intracellular channel 6 (CLIC6), J. Biol. Chem. 299 (2023) 105349.
[28] H. Zhou, Y. Xi, X. Chen, Chloride intracellular channel 6 inhibits hepatocellular carcinoma progression by modulating immune cell balance and promoting tumor cell apoptosis, Cytojournal. 22 (2025) 20.
[29] K. Fahima, M.R. Hosen, Z. Mahmud, Comprehensive epigenomic and transcriptomic analysis identifies FABP7 and CLIC6 as methylation-driven prognostic biomarker for a novel breast cancer subtype, Comput. Biol. Med. 201 (2026) 111430.
[30] J. Wang, Y. Wang, H. Ma, Y. Li, J. Hou, J. Li, et al., CLIC6's role in cancer: from broad analysis to breast cancer validation, Front. Oncol. 15 (2025) 1667589.
[31] M. Suo, L. Liu, T. She, C. Chen, Targeting CLIC6 with theaflavin enhances radiotherapy sensitivity in ER+/HER2- breast cancer, Transl. Cancer Res. 14 (2025) 9002–9014.
[32] Y.-Q. Zhou, X.-X. Cheng, S. He, S.-Q. Liu, Y.-Q. Li, P.-P. Wei, et al., A positive feedback loop between PLD1 and NF-κb signaling promotes tumorigenesis of nasopharyngeal carcinoma, J. Genet. Genomics. 51 (2024) 997–1006.
[33] S. Xin, L. Liu, Y. Li, J. Yang, L. Zuo, P. Cao, et al., Cyclophilin A binds to AKT1 and facilitates the tumorigenicity of Epstein-Barr virus by mediating the activation of AKT/mTOR/NF-κb positive feedback loop, Virol. Sin. 37 (2022) 913–921.
[34] PLOS Genetics Editors, Expression of concern: NKILA represses nasopharyngeal carcinoma carcinogenesis and metastasis by NF-κb pathway inhibition, PLoS. Genet. 18 (2022) e1010332.
[35] X. Zhou, L. Matskova, S. Zheng, X. Wang, Y. Wang, X. Xiao, et al., Mechanisms of anergic inflammatory response in nasopharyngeal carcinoma cells despite ubiquitous constitutive NF-κb activation, Front. Cell Dev. Biol. 10 (2022) 861916.
[36] S. Li, G. Pi, Y. Zeng, C. Ruan, X. He, X. Xiong, et al., Notoginsenoside R1 induces oxidative stress and modulates LPS induced immune microenvironment of nasopharyngeal carcinoma, Int. Immunopharmacol. 113 (2022) 109323.
[37] Y. Wang, Y. Chen, Y. Liu, J. Zhao, G. Wang, H. Chen, et al., Tumor vascular endothelial cells promote immune escape by upregulating PD-L1 expression via crosstalk between NF-κb and STAT3 signaling pathways in nasopharyngeal carcinoma, Cell Death. Dis. 16 (2025) 129.
[38] J. Chen, N. Liu, Q. Tao, J. Wu, J. Huang, C. Lu, et al., Vinburnine sensitizes radiotherapy efficacy in nasopharyngeal carcinoma by triggering pyroptosis and immune responses via activation of EDAR-nfκb pathway, Adv. Sci. (Weinh) 12 (2025) e06139.